American Mineralogist, Volume 82, pages 549–556, 1997

The solubility of H_2O in phonolitic melts

MICHAEL R. CARROLL[1] AND JENNIFER G. BLANK[2]

[1]Department of Geology, Bristol University, Bristol BS8 1RJ, U.K.
[2]Geophysical Laboratory, Carnegie Institution of Washington, 5451 Broad Branch Road NW Washington, DC 20008 U.S.A.

ABSTRACT

We have calibrated the IR spectroscopic technique for measurement of H_2O dissolved in phonolitic glasses as hydroxyl and H_2O molecules using manometric and weight-loss methods. The resulting molar absorptivity coefficients are $1.25^{+0.33}_{-0.22}$ (for absorbance due to OH^- at 4500 cm^{-1}) and $1.10^{+0.12}_{-0.10}$ (for absorbance due to molecular H_2O at 5200 cm^{-1}). These values are similar to those previously determined for hydrous jadeitic glasses. We have applied our calibration to a new set of solubility experiments in which H_2O and a natural phonolitic glass were equilibrated at near-liquidus temperatures (85–973 °C) and pressures of 191–1500 bars for periods of 38–272 h. We used a regular solution model to develop an equation of state for the solubility of H_2O in phonolitic melts. Our experimental results demonstrate that H_2O solubility is appreciably higher in phonolitic melts compared with basaltic and rhyolitic melts at the same pressures and near-liquidus temperatures; e.g., the solubility of H_2O at 1000 bars is 4.9 wt% in phonolitic melt (850 °C), 4 wt% in rhyolitic (850 °C), and 3.2 wt% in basaltic (1200 °C) melts. The calculated partial molar volume of dissolved H_2O in phonolitic melt (8.5 ± 2.5 cm^3/mol) falls between that determined by similar methods for rhyolitic and basaltic melts, but we note that the significance of this number is unknown because speciation changes during quenching are not sufficiently well characterized.

INTRODUCTION

Exsolution of dissolved H_2O during magma decompression provides a major driving force for subaerial explosive volcanism. To construct quantitative models of magmatic systems and eruptive processes it is desirable to know the variation of H_2O solubility with changes in melt composition, pressure, and temperature. In general, experimental data document a strong pressure dependence of H_2O solubility (e.g., from ~0.1 wt% at 1 bar, to ~1 wt% at 100 bars, to ~3–5 wt% at 1000 bars) and much smaller, negative temperature dependence, on the order of a few tenths of a weight percent over several hundreds of degrees at near-liquidus temperatures (Holtz et al. 1992). The effect of melt composition on H_2O solubility is less understood and not easily predicted with great accuracy. Burnham (1979, 1981) introduced an H_2O solubility model that accounts for changes in melt composition, and although his model works well for silicic melts there are considerable discrepancies between measured and predicted solubilities for other compositions (cf., Holloway and Blank 1994). Moore et al. (1995) proposed an empirical model for calculating the effects of melt composition, *P*, and *T* on H_2O solubility that appears to work well for calc-alkaline magma compositions but whose applicability to a wider range of compositions remains to be determined.

While H_2O solubilities in rhyolitic and basaltic melts are relatively well known at pressures up to several thousand bars (Hamilton et al. 1964; Silver et al. 1990; Blank et al. 1993; Dixon et al. 1995), high quality measurements of H_2O solubilities in diverse natural melt compositions are not abundant (Holloway and Blank 1994). Some data exist for H_2O dissolved in andesitic (Hamilton et al. 1964) and basanitic (Cocheo and Holloway 1993) compositions, and Moore et al. (1995) have recently presented 16 bulk H_2O solubility determinations in 7 natural melt compositions at pressures below 2 kbar. Among what might be broadly classified as rhyolitic melt compositions, systematic variations exist in H_2O solubility, and these variations are sensitive to changes in the proportions of Na and K (Holtz et al. 1994); there is generally a higher H_2O solubility in more Na-rich melts. There are also numerous solubility determinations for a wide variety of simple synthetic melt compositions (cf. McMillan 1994), but extrapolation from these results to natural melt compositions is not straightforward.

Recent studies of the alkaline volcanism of Teide volcano (Tenerife, Canary Islands) has spurred our interest in the behavior of H_2O in phonolitic melts. The absence of existing experimental data and uncertain accuracy of available H_2O solubility models prompted us to determine a new FTIR calibration for measurement of hydrous species in phonolitic glasses directly. These results have been used to determine H_2O solubility behavior in a relatively evolved phonolitic-melt composition, synthesized under H_2O-saturated conditions at near liquidus temperatures

0003–004X/97/0506–0549$05.00

TABLE 1. Phonolite starting compositions (wt%)

	T2-182	T1-214a	JD-idl	D-PHO
SiO_2	59.38	59.50	59.45	58.7
Al_2O_3	18.92	18.72	25.22	24.5
TiO_2	0.66	0.63		
Fe_2O_3*	3.85	3.85		
MgO	0.33	0.33		
CaO	0.79	0.78		
Na_2O	10.07	9.98	15.33	11.3
K_2O	5.55	5.43		5.5
MnO	0.2	0.2		
P_2O_5	0.07	0.08		
LOI	0.45	0.28		
Total	100.04	99.7	100.	100.

Notes: T2-182 and T1-214a are 2 phonolitic obsidian fragments from the Montaña Blanca pumice deposit, Tenerife, Canary Islands. Their XRF analyses above are normalized to 100% anhydrous melt. Totals listed are not normalized and include trace element contributions, primarily Cl (3350 ppm), F (860 ppm), and Zr (1122 ppm). The molecular weight on a per O atom basis of dry T2-182 phonolite, assuming 2% FeO and 2% Fe_2O_3, is 34.874. Included for comparison are JD-idl, the composition of $NaAlSi_2O_6$ calculated from stoichiometry, and D-PHO, the normalized anhydrous composition of the melt studied by Dingwell et al. (1984), which contained 5.01 wt% H_2O.

* Total iron as Fe_2O_3; LOI = Loss on ignition.

(850–973 °C) and total pressures up to 1500 bars. The results contribute to our general understanding of how H_2O solubility varies with melt composition and facilitate the quantitative use of FTIR spectroscopy to measure the concentration and speciation of H_2O in natural phonolitic glasses and melt inclusions.

EXPERIMENTAL AND ANALYTICAL METHODS

Starting materials

Experiments were performed using natural peralkaline phonolitic glass collected from the 2020 years old subunit IIA of the Montaña Blanca pumice deposit (Tenerife). Chemical analyses of two hand-sized samples of the obsidian used as starting material are given in Table 1. Chemically indistinguishable, the samples consist of 96–99 vol% fresh, dark-green glass and 1–4 vol% euhedral phenocrysts. Feldspar is modally dominant (~90%), and other phases, in order of decreasing abundance, are sodic clinopyroxene, biotite, magnetite, ilmenite, and apatite.

Starting materials were prepared in two forms. A fine-grained powder of 50–100 μm grain size was prepared from obsidian crushed using an agate mortar and pestle. Cylindrical cores (3 mm diameter, 5–10 mm length) were drilled using a diamond coring bit from sectioned obsidian slabs ~10 mm thick submerged in water. Both types of sample material were rinsed in a sonicated ethanol bath, dried in air, and stored in clean glass bottles before use.

Experiments

Approximately 50–100 mg of sample and 3–10 mg of distilled, deionized water were welded inside 3 mm diameter gold capsules. Several additional capsules were prepared using 2 mm diameter $Ag_{70}Pd_{30}$ tubing (RG sample numbers in Table 2). Capsule weight was monitored using an electronic balance throughout the loading process and all samples showed no weight loss after welding and subsequent heating to 110 °C. The amount of water sealed along with glass inside of a capsule varied according to the desired experiment pressure and was kept at a minimum, from 3–10% by weight of the total material loaded into capsules, to avoid changes in sample composition because of solubility of silicate components in the fluid phase. Normalized microprobe analyses of selected samples following their exposure to elevated pressure and temperature were indistinguishable, and we concluded that the solution of melt components in the fluid phase did not noticeably alter the compositions of the phonolitic melts.

Experiments were conducted in rapid-quench, water-pressurized cold-seal vessels consisting of a Nimonic 105 vessel connected to a 30 cm long stainless steel extension by means of a water-cooled coupling nut. The entire vessel had an internal bore diameter of 6.35 mm. The sample holder consisted of a magnetically levitated stainless-steel rod with an Inconel cup at one end, into which the sample capsule was placed. Samples were held in position within the hot zone of the furnace by means of a donut-shaped cylindrical magnet fit over the stainless-steel extension to the pressure vessel. Quenching was accomplished by rapidly lowering the magnet to the base of the stainless-steel extension, causing the sample support rod to drop and the capsule to be lowered to the center of the water-cooled coupling piece. We have not measured quench rates in these vessels but in TZM vessels of similar design it takes 2–3 s for a thermocouple, initially resting at 1100 °C, to cool to 25 °C after being lowered into the water-cooled coupling piece (Blank 1993). Samples, being of large mass, experienced slower quenching yet probably cooled at rates greater than 100 °C/sec.

The samples were held at elevated temperatures and pressures for times ranging from 38–272 h. Experimental conditions varied from 850–973 °C and 191–1500 bars (Table 2). Lower-pressure experiments were conducted at temperatures > 900 °C to avoid crystallization of the phonolitic melt. The experimental procedure involved first pressurizing the sample to approximately half of the desired final pressure, then heating the sample and bleeding pressure as it rose due to temperature increase, keeping the pressure 100 to 200 bars below the desired final pressure until the sample reached the desired temperature. Pressure was then increased by pumping to achieve the desired final value. This procedure was important for producing bubble-free samples in experiments using glass cores as starting material, and for consistency the same approach was used for experiments with powdered starting materials. Quenching was accompanied by a pressure rise of ~300 bars as the metal in the hot zone of the furnace was replaced by water.

Following quenching, experimental charges were removed from the pressure vessel, dried, weighed, and then punctured using a needle. Excess water inside the capsule, present in all experimental charges used to deter-

TABLE 2. Experimental runs, conditions, and results

Run No.	Start material*	Duration (h)	*P* (bars)	*T* °C	OH (wt%)†	H_2O (molec)‡	H_2O total§	n	Abs_{4500} (per cm)	Abs_{5200} (per cm)	Density (g/l)	Thickness (μm)	Notes
R129	MBP-c	120h	191	973	0.83(2)‖	0.44(1)	1.27(2)	3	1.399	0.655	2431	360	
R127	MBP-c	168h	250	900	0.96(3)	0.80(1)	1.76(4)	6	1.616	1.181	2424	345	[1]
RG59	MBP-p	168h	290	875	0.97(2)	1.24(2)	2.21(3)	3	1.637	1.812	2417	142	
R130	MBP-p	144h	330	925	1.01(1)	1.22(5)	2.23(5)	3	1.705	1.782	2417	185	
R105	MBp-c	38h	360	900	1.13(5)	1.31(7)	2.44(5)	5	1.896	1.922	2413	141	
R105							2.40(15)		weight loss				
R124	MBP-c	120h	500	860	1.25(1)	1.76(4)	3.01(4)	4	2.094	2.565	2405	246	[2]
R124	19.50 mg sample, 25.72 μmol H_2 yield						2.38(10)		manometry				[3]
R116	MBP-c	120h	560	875	1.21(1)	1.73(3)	2.94(4)	3	2.030	2.520	2406	119	[4]
R116	19.50 mg sample, 31.68 μmol H_2 yield						3.00(10)		manometry				[4]
R104	MBP-p	48h	600	875	1.30(2)	2.28(1)	3.58(3)	2	2.176	3.307	2396	88	
R166	MBP-c	58h	700	885	1.19(2)	2.70(2)	3.89(3)	4	1.979	3.920	2392	520	[5]
R166							3.85(15)		weight loss				
R94	MBP-p	72h	750	850	1.16(5)	3.22(10)	4.38(13)	5	1.919	4.659	2384	154	[5]
R119	MBP-c	144h	950	850	1.35(5)	3.24(7)	4.59(6)	5	2.244	4.669	2381	353	
R128-r	MBP-p	144h	960	875	1.51(3)	3.21(3)	4.72(5)	6	2.495	4.630	2379	466	[6]
R100	MBP-p	96h	1000	850	1.35(8)	3.67(3)	5.02(11)	3	2.232	5.284	2374	145	
RG35	MBP-p	125h	1000	875	1.52(17)	3.05(21)	4.57(10)	6	2.519	4.399	2381	234	
R99	MBP-p	96h	1025	850	1.90(7)	3.20(1)	5.10(5)	3	3.135	4.603	2373	63	
R117	MBP-c	144h	1025	850	1.41(2)	3.59(6)	5.00(8)	6	2.316	5.168	2375	185	[2]
R117	36.44 mg sample, 85.38 μmol H_2 yield						4.22(10)		manometry				[3]
R165	MBP-p	96h	1230	880	1.40(3)	4.02(20)	5.42(22)	6	2.314	5.761	2369	173	
R125	MBP-c	120h	1410	850	1.45(4)	3.812(4)	5.27(4)	4	2.396	5.470	2371	193	[7]
R125	13.92 mg sample, 40.70 μmol H_2 yield						5.23(10)		manometry				[3]
R91	MBP-p	168h	1480	850	1.64(6)	4.59(4)	6.23(9)	4	2.691	6.539	2357	388	
RG62	MBP-p	272hr	1500	870	1.49(5)	4.84(13)	6.33(17)	9	2.449	6.906	2355	190	

Notes: [1] Used part of experiment previously run at 900 °C, 200 bars, but which was partially crystalline. [2] Portions of sample had microlites. [3] Manometry measurements done by U reduction as described in text. [4] Some irregularly distributed bubbles, <10 μm diameter. [5] Sample run in conventional, air-quench pressure vessel (slower quench); not used in speciation modeling. [6] Reversal experiment, held initially at 1635 bars for 2 days before being equilibrated at indicated conditions. [7] H_2O undersaturated experiment; no excess H_2O present when capsule was opened; not used in modelling pressure dependence of solubility but included in modeling of speciation. Densities calculated iteratively using measured water contents, anhydrous density of 2450 g/l, and assumed density decrease of 15 g/l per weight percent H_2O in sample (average from Silver et al. 1990 results).

* Starting materials include p = powder, c = core.

† OH^- as H_2O weight percentage, from 4500 cm^{-1} absorbance intensity.

‡ Molecular H_2O, wt%, from ~5200 cm^{-1} absorbance intensity.

§ Total H_2O, wt%, from sum of OH^- and molecular H_2O.

‖ Error on measurements, from 1σ standard deviation on total number of measurements (n).

mine H_2O solubility, provided evidence that experiments were conducted under H_2O-saturated conditions. The amount of excess H_2O was determined by heating punctured capsules for ~5 min at 110 °C, and reweighing to check for H_2O evaporation. Afterwards, capsules were torn open with pliers and fragments from each sample were mounted in orthodontic resin and prepared as doubly polished glass chips for IR spectroscopic analysis. The thicknesses of the polished samples were determined to ±1 μm using a Mitutoyo digital displacement gauge. Aliquots of bubble-free material from selected samples were also set aside for bulk analysis by vacuum fusion-manometry or weight-loss.

Infrared spectroscopy

The doubly polished glass chips from the experiments were cleaned ultrasonically in acetone and ethanol and examined under a petrographic microscope before analysis. Transmission FTIR spectra at 4 cm^{-1} resolution were collected for 512–1024 scans using a Spectratech FTIR microscope (15× objective) and Nicolet Model 800 FTIR spectrometer configured with a CaF_2 beamsplitter, a visible light source, and an MCT (HgCdTe) detector.

Polished samples were situated under the microscope objective in several different ways. Glass chips were placed over millimeter-sized holes in lead foil, and a 100 μm aperture was centered over a clear, glassy region in the sample free of bubbles and cracks; 3–9 separate spots were analyzed on each sample to check for homogeneous H_2O distribution. For some of the smallest samples (e.g., broken during polishing), spectra were collected while the samples rested on IR-transparent KBr or NaCl windows (2 mm thick); results from these measurements were indistinguishable from those obtained from samples resting directly on holes in metal foil. Several samples were also analyzed using the main sample compartment of the FTIR and a second MCT detector, with samples positioned over 300 μm apertures. No differences in absorbance intensities were detected between spectra collected using these two configurations.

Infrared peaks corresponding to vibrations involving H_2O molecules (~5200 cm^{-1}) or hydroxyl groups (~4500 cm^{-1}) were used to determine H_2O speciation and total dissolved concentrations (cf., Stolper 1982). Background-corrected absorbances for these bands were determined by measuring the intensities of the absorptions at ~4500 and 5200 cm^{-1}; total H_2O content was determined from the sum of the contributions from the two species. Ab-

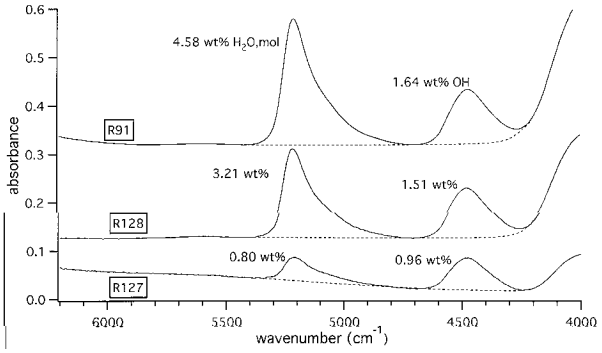

FIGURE 1. Representative FTIR spectra of three phonolitic glasses with 1.76, 4.72, and 6.22 wt% total dissolved H_2O; see Table 2 for synthesis conditions. Approximate backgrounds are indicated with dashed lines, and numbers next to peaks are calculated quantities of molecular H_2O (5200 cm^{-1}; $\epsilon_{5200} = 1.10$) and hydroxyl (4500 cm^{-1}; $\epsilon_{4500} = 1.25$). Spectra have been normalized to a 400 μm sample thickness.

solute absorbances of these bands were in all cases below 0.5, within the range of linear detector response. Backgrounds were generally flat (Fig. 1) and easy to determine. The band at ~3550 cm^{-1} was saturated as a result of the high H_2O concentrations and chosen sample thicknesses. We did not use the first overtone of this band at ~7100 cm^{-1} because of its poor resolution, resulting from either poor signal-noise or because in some samples this peak occurred on the limb of a broad-absorption band associated with Fe^{2+} centered near 9500 cm^{-1}.

Vacuum fusion and H_2O extraction

H_2O contents of aliquots of four glass samples were determined using the conventional uranium method (Bigeleisen et al. 1952), in which H_2O liberated by heating a sample is converted quantitatively to H_2 by reaction with hot uranium. Results were correlated with the infrared spectroscopic measurements and used to calibrate the IR technique for direct quantitative measurement of dissolved H_2O species.

The vacuum fusion measurements were initiated by placing a platinum crucible containing a known amount of sample material (~0.5–2 mm sized chips) in the induction furnace-extraction line and heating overnight at 150 °C. Further heating at 300 °C for 30 min released a negligible amount of H_2O. Samples were subsequently subjected to two 40 min combustions at 600 °C and 900 °C, during which time the bulk of the H_2O was released. A final 30 min combustion at 1400 °C provided a check for complete extraction of dissolved H_2O; in all cases only a small proportion of the total H_2O was collected from this temperature interval. During heating, glass samples were exposed to O_2 (≈ 5.5 torr) from a CuO furnace at 895 °C to ensure complete oxidation of liberated gases, which were condensed directly into a liquid nitrogen (−190 °C) trap. After each combustion interval, carbon dioxide was distilled from water cryogenically with a −110 °C slurry of dry ice and ethanol; the water ice remaining was evaporated and then converted to H_2 by being passed twice over hot uranium at 895 °C. Hydrogen gas was transferred to a mercury manometer with a Toepler pump and measured to obtain a quantitative yield. H_2 yield was measured after each temperature step and the sample's H_2O concentration was determined from the cumulative totals collected for temperature steps ≥600 °C. A procedural blank of ~5 μmol H_2 was determined before each sample extraction, and yields were corrected accordingly.

Weight-loss measurement

The H_2O contents of two samples (R105, R166; Table 2) were measured by weight loss. This was done when it was not possible to make H_2 manometry measurements, which have a major advantage in terms of useful sample size (smaller) and precision. The glass cylinders from these experiments were cut in half, yielding bubble-free samples of ~50–75 mg, and these were crushed gently to millimeter-sized chips which were placed in a platinum tube with one sealed end and the top lightly crimped. The sample was weighed to a precision of 0.01 mg, placed in a furnace, and heated over ~6 h to 1000 °C. It was then removed, weighed, placed in the furnace at 1000 °C for 1 h, reweighed, heated at 1250 °C for one hour, and weighed a final time. Neither of the last two steps produced any change in weight. The measured weight loss for these samples corresponds to H_2O contents of 2.2 and 3.75 wt%. If we assume that all the Fe in the sample was oxidized to Fe_2O_3 the calculated H_2O contents are 2.4 and 3.95 wt%. With no additional data available, we have assumed that all of the Fe was oxidized to Fe^{3+} (the glasses were red-colored) and have assumed that the correct H_2O contents are 2.4 ± 0.15 and 3.85 ± 0.15 wt%. The large sample mass required to counterbalance weighing errors precluded measurement of additional samples using this technique.

Calibration of molar absorptivities

Quantitative measurement of H_2O concentration using IR spectroscopy requires calibration of the molar absorptivities of the bands of interest for the melt composition of interest (Stolper 1982b; Newman et al. 1986). The Beer-Lambert law provides the basis for the quantitative relation between absorption intensity and species concentration:

$$c = \frac{18.015A}{\rho t \epsilon} \quad (1)$$

where c is the H_2O concentration (in weight fraction), 18.015 is the molecular weight of H_2O, A is the height of the absorbance peak, t is the sample thickness, ρ is the sample density (g/l), and ε is the molar absorptivity [or extinction coefficient; in l/(mol·cm)]. For samples in which the total H_2O content can be described as the sum as molecular and hydroxyl species, we can rewrite Equation 1 as

$$c_{\text{total}} = \frac{1}{\epsilon_{4500}}\left(\frac{18.015A_{4500}}{\rho t}\right) + \frac{1}{\epsilon_{5200}}\left(\frac{18.015A_{5200}}{\rho t}\right) \quad (2)$$

where A_{4500}, A_{5200} refer to absorbances at ~4500 and 5200 cm^{-1}, and ϵ_{4500}, ϵ_{5200} refer to the molar absorptivities of these bands; the band at ~4500 cm^{-1} (average at 4477 cm^{-1} in our measurements) corresponds to H_2O present as hydroxyl groups, and the band at ~5200 cm^{-1} (average at 5212 cm^{-1} in our measurements) corresponds to H_2O present as molecular H_2O species (Stolper 1982b; Silver et al. 1990). Given at least two samples with different total H_2O contents (determined by independent means) it is possible to solve Equation 2 for the unknown values of ϵ_{4500} and ϵ_{5200} using multiple linear regression. The densities of the hydrous glasses were estimated using the procedure of Lange and Carmichael (1987) and then corrected for the effect of H_2O assuming that density decreased by 15 g/l per wt% dissolved H_2O present (cf. Silver et al. 1990).

Using our bulk analysis data and FTIR measurements on the same samples (experiments R125, R116, R105, and R166), we have determined best-fit molar absorptivity values of $\epsilon_{4500} = 1.25^{+0.33}_{-0.22}$ and $\epsilon_{5200} = 1.10^{+0.12}_{-0.10}$. The quoted errors are statistical errors derived from the covariance matrix of the multiple linear regression fit, with all samples given equal weighting in the fit. The measured total H_2O contents were fit well with the assumption of constant-valued molar absorptivities; the mean difference between bulk analysis results and values calculated from the multiple linear regression is 0.03 wt% H_2O (range from 0.06 to 0.01 wt% H_2O).

Two additional samples (R124 and R117; see Table 2) were also analyzed by manometry but were not included in the calibration because subsequent examination of multiple glass chips from these samples showed that some contained irregular masses of very fine oxides and a low birefringence mineral, probably feldspar; macroscopically these crystal-bearing chips did not look different from crystal-free chips. We can only surmise that some of the chips chosen for manometry from these samples contained crystals, thus yielding low total H_2O concentrations. The presence of oxide minerals suggests that oxidation-induced crystallization of oxide minerals may have driven the liquid to saturation in feldspar, as the experiments are close to the phonolite liquidus. As shown below, FTIR measurements on crystal-free portions of these samples give results in good agreement with those of other experiments done at similar pressures.

The uncertainties in the molar absorptivities are most strongly influenced by the small range of OH contents in the samples analyzed, hence the larger error associated with the best-fit ϵ_{4500}. Considering the similar concentrations of silica, alumina, and total alkalis (Table 1) in the phonolitic composition we have studied and the jadeitic composition investigated by Silver et al. (1990), it would be surprising if the molar absorptivities for these two compositions differed greatly (e.g., see discussion of correlations between molar absorptivities and melt composition in Dixon et al. 1995). We have calculated total H_2O concentrations in three jadeitic glasses studied by Silver et al. (1990) and find that they can be reproduced to within 0.1 wt% H_2O using our best-fit phonolite ϵ_i values. In fact, the fit uncertainties render our calculated molar absorptivities for phonolite indistinguishable from the values $\epsilon_{4500} = 1.12$ and $\epsilon_{5200} = 1.13$ reported by Silver et al. (1990) for H_2O in jadeitic glasses.

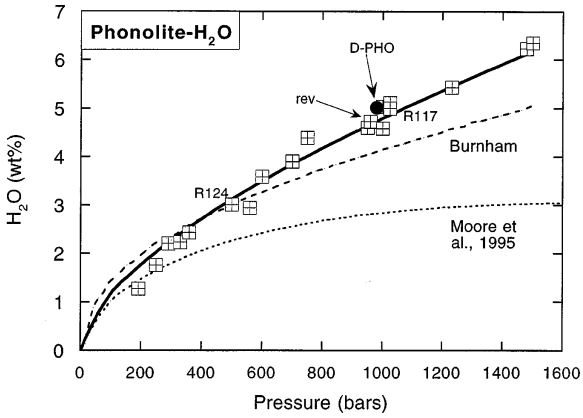

FIGURE 2. The variation of H_2O solubility in phonolitic melts as a function of pressure. Data from FTIR analyses; 'rev' indicates a reversal experiment (see text). H_2O contents are the sum of H_2O as molecular and hydroxyl species, determined from absorbance band intensities at ~5200 cm^{-1} and ~4500 cm^{-1}, respectively, using our new calibration. Closed circle (D-PHO) indicates H_2O solubility determined by Dingwell et. al. (1984) for a synthetic phonolitic melt with composition similar to the one we have used (see Table 1; experiment at 970 bars, 800 °C, analyzed by vacuum extraction). The two samples for which manometric analysis gave low H_2O concentrations, because of the presence of crystals, are indicated (R124 and R117; see text for discussion); the plotted IR results for crystal-free portions of these samples are in good agreement with other results. Solid curve indicates the calculated H_2O solubility as a function of pressure at 850 °C, using Equations 3 and 4; dashed curves show predicted solubilities in phonolitic melt on the basis of models of Burnham (1981) and Moore et al. (1995). Note that the solubility data can also be fit with a power law (percent $H_2O = 0.0329 \cdot P^{0.7238}$; pressure in bars).

RESULTS

Solubility

Our new IR calibrations for molar absorptivities of molecular and hydroxyl species in hydrous phonolitic glasses were applied to measuring the concentrations of H_2O dissolved in phonolitic glasses quenched from H_2O-saturated melts at high T and P. The relation between total H_2O solubility and pressure, over the range of our experimental conditions, is depicted in Figure 2. A reversal experiment, held initially at 1635 bars for 48 h before lowering the pressure to 960 bars and holding for 144 h yields results in excellent agreement with other experiments. The FTIR results on crystal-free glass chips of the two manometrically analyzed samples that gave low results (R124, R117) are in good

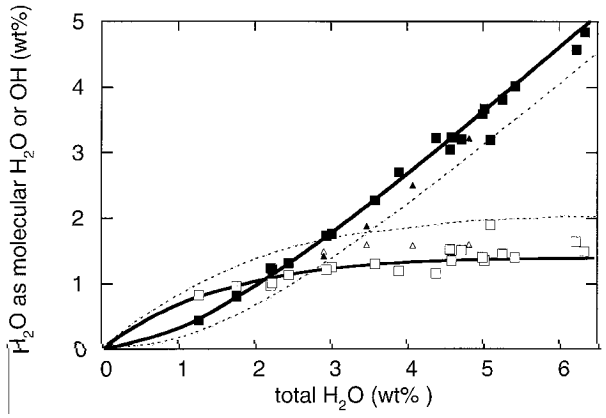

FIGURE 3. H_2O speciation as a function of total H_2O content. Open and closed symbols indicate hydroxyl and molecular H_2O, respectively; squares are phonolite data (this study), triangles are jadeite data (Silver et al. 1990). Solid curves are model speciation for phonolitic glass, on the basis of fit of data to Equation 4 as described in text. Dashed curves show Dixon et al. (1995) model speciation data for hydrous basaltic glass quenched from 1200 °C.

agreement with the solubility trend defined by the other data, in support of our belief that the manometrically determined H_2O contents for these samples are too low, probably because of the presence of fine grained oxide + feldspar crystals in some glass chips used for manometry. The solid curve passing through the data in Figure 2 is the calculated variation in solubility with pressure at 850 °C, on the basis of a regular solution model fit of the data (Silver and Stolper 1985; 1989) discussed below. Our results agree well with a previous determination of H_2O solubility in a phonolitic composition at a single pressure and temperature (Dingwell et al. 1984).

The two dashed curves in Figure 2 show calculated H_2O solubilities in phonolitic melt on the basis of the models of Burnham (1981) and Moore et al. (1995). Both of these models underestimate H_2O solubilities, with the Burnham model to a lesser degree. Upon applying our calibration to IR data on water-saturated samples of Moore et al. (1995), however, we find excellent agreement with our solubility results. G. Moore (personal communication) who based his solubility determinations on manometric analyses as well, has suggested that his samples may have suffered water loss during low-temperature evacuation for extended periods before extraction at high temperatures.

Speciation

The speciation of H_2O in hydrous phonolitic glasses varies with total H_2O content in a manner typical of many other silicate compositions. The proportions of H_2O present as hydroxyl groups and as H_2O molecules in hydrous phonolitic glasses are plotted as a function of total H_2O content in Figure 3, along with speciation data for hydrous jadeitic glasses (Silver et al. 1990) and model curves (dashed) showing H_2O speciation in hydrous basaltic glass (Dixon et al. 1995). Samples with total H_2O contents less than 1–2 wt% have OH^- as the dominant species, but with increasing total H_2O the samples show an increasing abundance of molecular H_2O and approximately constant hydroxyl concentration, similar to previously published results for hydrous glasses (Bartholomew et al. 1980; Stolper 1982a,b; Silver et al. 1990). In comparison with published results for hydrous basaltic, rhyolitic, and albitic glasses, H_2O speciation in phonolitic samples generally shows less hydroxyl and more molecular H_2O at a given total H_2O content. The relative proportions of molecular and hydroxyl H_2O present in the quenched samples may not reflect the speciation in the melt at the elevated temperatures and pressures of the experiments, but without knowledge of how speciation varies with quench rate, or in situ measurements, it is not possible to be more quantitative about speciation in high-temperature melts (Silver et al. 1990; Dingwell and Webb 1990; McMillan 1994; Zhang et al. 1995; Nowak and Behrens 1995).

Solubility model

Previous spectroscopically based studies of H_2O solubility and speciation in a variety of quenched melt compositions have shown that the solubility behavior for a given melt composition can be modelled using a relatively simple thermodynamic approach that considers the hydrous melt to consist of H_2O molecules, OH groups, and O atoms involved in coordination of the cations present in the melt (Silver and Stolper 1985, 1989; Silver et al. 1990). If the activity of H_2O in vapor-saturated melt is assumed to be proportional to the mole fraction of molecular H_2O present in the quenched glasses, then the variation in H_2O activity with pressure and temperature is given by

$$\ln\left(\frac{a^{m}_{H_2O,mol}(P_2, T_2)}{f^{o}_{H_2}(P_2, T_2)}\right) = \ln\left(\frac{a^{m}_{H_2O,mol}(P_1, T_1)}{f^{o}_{H_2O}(P_1, T_1)}\right) - \frac{V^{o,m}_{H_2O}(P_2 - P_1)}{RT_2} - \frac{\Delta H^{o}_{H_2O}}{R}\left(\frac{1}{T_2} - \frac{1}{T_1}\right) \quad (3)$$

where P_1, T_1 and P_2, T_2 refer to two sets of vapor-saturated conditions, with P_1, T_1 taken as the reference conditions (1 bar, 850 °C for this work); $f^{o}_{H_2O}$ refers to the fugacity of pure H_2O at conditions P_1T_1 or P_2T_2; $V^{o,m}_{H_2O}$ is the molar volume of H_2O in the melt in its standard state; and $\Delta H^{o}_{H_2O}$ is the standard state enthalpy change for dissolution of H_2O vapor in the melt. This formulation predicts a simple linear proportionality between H_2O fugacity and H_2O activity at low pressures, where Henry's law applies, and the deviation from linear behavior at higher pressure is accounted for by the $V^{o,m}_{H_2O}$ term. Figure 4 shows that we observe such behavior for hydrous phonolitic glasses quenched from pressures up to 1500 bars. The solid curve in Figure 4 is the predicted variation in X_{H_2Omol} at 850 °C,

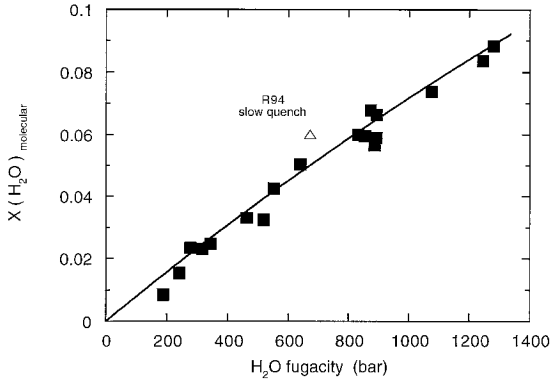

FIGURE 4. Variation of mole fraction of molecular H_2O (X_{H_2Omol}) dissolved in phonolitic glasses as function of f_{H_2O} for H_2O-saturated experiments. H_2O fugacities were calculated using the modified Redlich-Kwong equation of state (Holloway 1977). Solid curve indicates values calculated on the basis of a least-squares regression for the data applied to Equation 3. Experiment R94 was done in a conventional air-quench cold-seal vessel and the slow quenching yields a higher abundance of molecular H_2O in comparison with that observed for rapid-quenched samples with similar total H_2O contents.

TABLE 3. Phonolite-H_2O regular solution model parameters

Solubility parameters	
$\ln \frac{X^0_{H_2O,mol}}{f^0_{H_2O}}$	-9.439 ± 0.0345
$V^0_{H_2O}$	8.53 ± 2.52 (cm³/mol)
$\Delta H^0_{H_2O}$	$-4{,}294 \pm 1{,}540$ (cal/mol)
Speciation parameters	
$-\ln\left[\frac{X^2_{OH}}{(X_{H_2O,mol})(1 - X_{OH} - X_{H_2O,mol})}\right] = A' + B'X_{OH} + C'X_{H_2O,mol}$	
where $A' = 1.640 \pm 0.080$	
$B' = 13.91 \pm 2.74$	
$C' = 11.66 \pm 1.16$	

Notes: Reference conditions used for the calculations are $P_1 = 1$ bar, $T_1 = 850$ °C. Solubility data were fit using a multiple least-squares regression and each datum was weighted proportionally to the error that would be introduced by an uncertainty of ±0.1 wt% in molecular H_2O. For example, if an uncertainty of ±0.1 wt% in H_2O_{mol} gave an uncertainty in the ln (X/f) term above of ±0.1, the weighting factor would be 10 (e.g., see Bevington 1969). Speciation data were fit using the same weighting. Mole fractions were calculated on single O atom basis, as described in Silver et al. (1990).

on the basis of multiple least-squares regression of our solubility data, with mole fractions calculated on a single oxygen basis as described in Silver et al. (1990). The best-fit values of $X_{H_2O,mol}/f^o_{H_2O}(P_1,T_1)$, $V^{o,m}_{H_2O}$, and $\Delta H^o_{H_2O}$ are summarized in Table 3. The slight degree of curvature at high fugacities shown by the data in Figure 4 can be accounted for by a $V^{o,m}_{H_2O}$ of 8.5 ± 2.5 cm³/mol; additional results at higher f_{H_2O} could better constrain the calculated $V^{o,m}_{H_2O}$, but we did not obtain viable glasses from experiments quenched from higher pressures. The unknown degree to which species reequilibration occurs during quenching also makes it difficult to treat the calculated partial molar volume term as more than an adjustable parameter to be used in fitting the experimental data (i.e., its physical significance cannot be evaluated until the effects of quenching on speciation can be quantified).

To calculate total solubilities from the X_{H_2Omol} values provided by Equation 3 it is necessary to quantify how the amounts of molecular and hydroxyl H_2O vary as a function of total dissolved H_2O content. We have used the regular solution formulation described in Silver and Stolper (1989) and fit our measured speciation data to

$$-\ln\left(\frac{(X_{OH})^2}{(X_{H_2Omol})(1 - X_{OH} - X_{H_2Omol})}\right) = A' + B'\cdot X_{OH} + C'\cdot X_{H_2Omol} \quad (4)$$

where the parameters A', B', and C' are determined from multiple least-squares regression of the spectroscopically determined speciation data; the best-fit values of A', B', and C' determined from our data are given in Table 3. Using these values it is possible to calculate total H_2O solubilities by first calculating X_{H_2Omol} at the pressure of interest using Equation 3, and then calculating the corresponding value of X_{OH} through iterative solution of Equation 4. The ability of this approach to reproduce closely our experimental results is illustrated by the model curves plotted in Figures 2 and 3.

DISCUSSION

The effect of melt composition on H_2O solubility can be evaluated by comparison of our results with those published for other compositions. The higher solubility of H_2O in phonolitic melts than in basaltic and rhyolitic melts is illustrated in Figure 5. The dashed curves labeled rhyolite and basalt show H_2O solubilities in the indicated melt compositions. These data show that phonolitic melts are capable of incorporating a significantly higher pro-

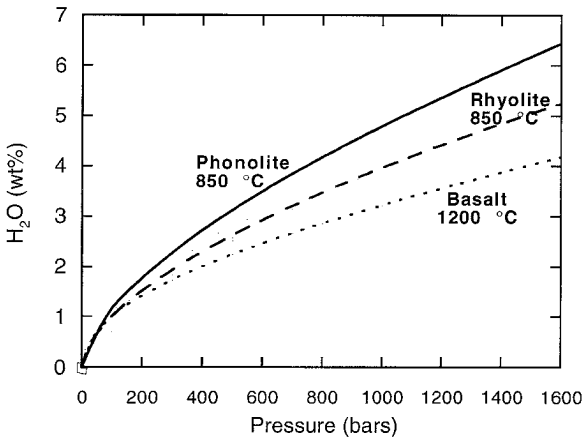

FIGURE 5. H_2O solubility in phonolitic compared with that in rhyolitic and basaltic melts. Curves denote model solubilities as discussed in text. Data sources are: phonolite, 850 °C, this study; rhyolite, 850 °C, Silver et al. 1990; basalt, 1200 °C, Dixon et al. 1995.

portion of dissolved H_2O at a given pressure than rhyolitic or balsaltic melts. The simplest consequence of the high measured H_2O solubilities in phonolitic melts is that for a given H_2O content, phonolitic magmas will be able to ascend to shallower depths in subvolcanic systems before becoming vapor saturated, or, if already vapor saturated, will be able to arrive closer to the surface with larger amounts of H_2O still dissolved in the melt.

Water speciation in the quenched phonolitic melts exhibits the same general behavior observed in previous spectroscopic studies of hydrous melts, but for a given total dissolved H_2O content, the phonolitic composition we have studied tends to have less hydroxyl and more molecular H_2O than found in basaltic and rhyolitic melts with the same total H_2O content. Whether this reflects a real difference in H_2O speciation in alkali-rich melts cannot be determined at present as it is clear that significant reequilibration may occur between molecular and hydroxyl species during quenching, and these quenching effects lead to an increased abundance of molecular H_2O in comparison with the amount originally present in the melt at high temperature (Stolper 1989; Silver et al. 1990; Zhang et al. 1995; Nowak and Behrens 1995). Although not complete, the available information concerning the kinetics of speciation reequilibration during quenching is sufficient to support the point of view that the $V^{o,m}_{H_2O}$, and $\Delta H^{o}_{H_2O}$ values determined from fitting of our solubility data may have little physical significance in terms of an atomistic understanding of the solution process in hydrous melts at elevated pressures and temperatures. Nonetheless, this approach to modeling H_2O solubility behavior does provide a useful means of quantitatively parameterizing the effects of P and T on the dissolved H_2O contents of natural magma compositions for which appropriate experimental solubility data exist.

Acknowledgments

This work was supported by the European Science Foundation, Environment Program, the NERC, and the Royal Society. We thank F. Wheeler and M. Overs for their expertise in the machine shop, and Z. Sharp and P. Agrinier for advice concerning analyses of H_2O in silicate materials using vacuum fusion techniques. J.G.B. acknowledges support from the Ministerie de la Culture et de l'Education de France and from the research program of C. Jaupart of the Laboratoire de Dymaniques des Systèmes Géologiques. M.R.C. acknowledges the hospitality and support of M. Pichavant and the CNRS, Orlèans, while the manuscript was being completed.

References cited

Bartholomew, R.F., Butler, B.L., Hoover, H.L., and Wu, C.K. (1980) Infrared spectra of a water-containing glass. Journal of the American Ceramic Society, 63, 481–485.

Bevington, P.R. (1969) Data Reduction and Error Analysis for the Physical Sciences, 336 p. McGraw-Hill, San Francisco.

Bigeleisen, J., Perlman, M.L., and Prosser, H.C. (1952) Conversion of hydrogenic materials to hydrogen for isotopic analysis. Analytical Chemistry, 24, 1356–1357.

Blank, J.G. (1993) An experimental investigation of the behavior of carbon dioxide in rhyolitic melt, Ph.D. thesis, California Institute of Technology.

Blank, J.G., Stolper, E.M., and Carroll, M.R. (1993) Solubilities of carbon dioxide and water in rhyolitic melt at 850 °C and 750 bars. Earth Planetary Science Letters, 119, 27-36.

Burnham, C.W. (1979) Magmas and hydrothermal fluids. In H.L. Barnes, Ed., Geochemistry of Hydrothermal Ore Deposits Vol. 2, p. 71–136. Wiley, New York.

———(1981) Nature of multicomponent aluminosilicate melts. In D.T. Rickard and F.E. Wickman, Eds., Chemistry and Geochemistry of Solutions at High Temperatures and Pressures, p. 197–229. Pergamon Press.

Cocheo, P.A. and Holloway, J.R. (1993) The solubility of water in basanitic melts at low pressures. Eos, 74, 350.

Dingwell, D.B. and Webb, S.L. (1990) Relaxation in silicate melts. European Journal of Mineralogy, 2, 427–449.

Dingwell, D.B., Harris, D.M., and Scarfe, C.M. (1984) The solubility of H_2O in melts in the system SiO_2-Al_2O_3-Na_2O-K_2O at 1 to 2 Kbars. Journal of Geology, 92, 387–395.

Dixon, J.E., Stolper, E.M, and Holloway, J.R. (1995) An experimental study of water and carbon dioxide solubilities in mid-ocean ridge basaltic liquids. Part I: Calibration and solubility models. Journal of Petrology, 36, 1607–1631.

Hamilton, D.L., Burnham, C.W., and Osborn, E.F. (1964) The solubility of water and effects of oxygen fugacity and water content on crystallization in mafic magmas. Journal of Petrology, 5, 21–39.

Holloway, J.R. (1977) Fugacity and activity of molecular species in supercritical fluids. In D. Fraser, Ed., Thermodynamics in Geology, p. 161–181. D. Reidel, Boston, Massachussets.

Holloway, J.R. and Blank, J.G. (1994) Application of experimental results to C-O-H species in natural melts. In Mineralogical Society of America Reviews in Mineralogy, 30, 187–230.

Holtz, F., Behrens, H., Dingwell, D.B., and Taylor, R.P. (1992) Water solubility in aluminosilicate melts of haplogranite composition at 2 kbar. Chemical Geology, 96, 289–302.

Holtz, F., Behrens, H., Dingwell, D.B., and Johannes, W. (1994) Water solubility in haplogranitic melts: Compositional, pressure, and temperature dependence. American Mineralogist, 80, 94–108.

Lange, R.A. and Carmichael, I.S.E. (1987) Densities of Na_2O-K_2O-CaO-MgO-FeO-Fe_2O_3-Al_2O_3-TiO_2-SiO_2 liquids: new measurements and derived partial molar properties. Geochimica et Cosmochimica Acta, 53, 2195–2204.

McMillan, P.F. (1994) Water solubility and speciation models. Mineralogical Society of America Reviews in Mineralogy, 30, 131–156.

Moore, G., Vennemann, T., and Carmichael, I.S.E. (1995) Solubility of water in magmas to 2 kbar. Geology, 23, 1099–1102.

Newman, S., Epstein, S., and Stolper, E.M. (1986) Measurement of water in rhyolitic glasses: Calibration of an infrared spectroscopic technique. American Mineralogist, 71, 1527–1541.

Nowak, M. and Behrens, H. (1995) The speciation of water in haplogranitic glasses and melts determined by in situ near infrared spectroscopy. Geochimica et Cosmochimica Acta, 59, 3445–3450.

Silver, L.A. and Stolper, E. (1985) A thermodynamic model for hydrous silicate melts. Journal of Geology, 93, 161–178.

———(1989) Water in albitic glasses. Journal of Petrology, 30, 667–710.

Silver, L.A., Ihinger, P.D., and Stolper, E. (1990) The influence of bulk composition on the speciation of water in silicate glasses. Contributions to Mineralogy and Petrology, 104, 142–162.

Stolper, E. (1982a) The speciation of water in silicate melts. Geochimica et Cosmochimica Acta, 46, 2609–2620.

———(1982b) Water in silicate glasses: an infrared spectroscopic study. Contributions to Mineralogy and Petrology, 81, 1–17.

———(1989) The temperature dependence of the speciation of water in rhyolitic melts and glasses. American Mineralogist, 74, 1247–1257.

Zhang, Y., Stolper, E.M., and Ihinger, P.D. (1995) Kinetics of the reaction $H_2O + O = 2\ OH$ in rhyolitic and albitic glasses: Preliminary results. American Mineralogist, 80, 593–612.

Manuscript received March 28, 1996
Manuscript accepted February 10, 1997